



Magnetism and local structure in low-dimensional Mott insulating GdTiO₃

Jack Y. Zhang,* Clayton A. Jackson,* Santosh Raghavan, Jinwoo Hwang, and Susanne Stemmer
Materials Department, University of California, Santa Barbara, California 93106-5050, USA

(Received 18 August 2013; published 16 September 2013)

Cation displacements, oxygen octahedral tilts, and magnetism of epitaxial, ferrimagnetic, insulating GdTiO₃ films sandwiched between cubic SrTiO₃ layers are studied using scanning transmission electron microscopy and magnetization measurements. With decreasing GdTiO₃ film thickness, structural (GdFeO₃-type) distortions are reduced, concomitant with a reduction in the Curie temperature. Ferromagnetism persists to smaller deviations from the cubic perovskite structure than is the case for the bulk rare-earth titanates. The results indicate that the ferromagnetic ground state is controlled by the narrow bandwidth, exchange and orbital ordering, and only to second order depends on the amount of the GdFeO₃-type distortion.

DOI: [10.1103/PhysRevB.88.121104](https://doi.org/10.1103/PhysRevB.88.121104)

PACS number(s): 71.27.+a, 68.37.Ma, 75.25.Dk

Perovskite rare-earth titanates are key materials to understand emergent phenomena caused by the coupling of the electron, lattice, spin, and orbital degrees of freedom. They are strongly correlated Mott insulators, with a single electron occupying the Ti t_{2g} orbitals. Magnetic ordering is closely coupled with distortions and tilts of the Ti-O octahedra in the orthorhombic GdFeO₃ structure (space group $Pbnm$) that all rare-earth titanates adopt, and which removes the orbital degeneracy.¹⁻³ Two distinct types of orbital polarization, namely, ferro-orbital and antiferro-orbital ordering, have been reported, and are compatible with $Pbnm$ symmetry.⁴⁻⁹ Ferro-orbital ordering is found in the antiferromagnetic (AFM) titanates, which also exhibit smaller GdFeO₃-type distortions ($A = \text{La} \dots \text{Sm}$ in the chemical formula $ATiO_3$), whereas antiferro-orbital ordering is found in the ferromagnetic (FM) titanates that also have larger distortions ($A = \text{Gd} \dots \text{Y}$).

The GdFeO₃ structure is characterized by $a^-a^-b^+$ -type octahedral tilts in Glazer notation.¹⁰ The two degrees of freedom in the $Pbnm$ space group (x and y) allow the A -site cations to shift to a more energetically favorable position. The amount of displacement depends on the octahedral geometry.¹¹ The degree of the GdFeO₃-type distortion appears to be a primary factor determining the transition from AFM to FM ordering, and the ordering temperature.^{1,3,12,13} Nevertheless, the relative roles of orbital-lattice coupling and structural distortions in this transition remain a subject of significant debate.^{6,12,14,15}

Epitaxial mismatch strains in heterostructures and the need for interfacial connectivity of the oxygen octahedra offer distinct and precise ways of tuning octahedral rotations and distortions without chemical substitution.^{16,17} This may allow for controlling orbital-lattice coupling, and thus the magnetic properties, as well as insights into materials physics not possible with bulk materials.

In this Rapid Communication, we report on the local structure and magnetism of GdTiO₃ films that are sandwiched between cubic SrTiO₃ with the goal to understand how rigidly the magnetic interactions are coupled to the octahedral tilts in a prototype FM rare-earth titanate. In GdTiO₃, the ferromagnetic Ti array couples antiferromagnetically to the Gd ions, resulting in net ferrimagnetism.^{12,13,18} The AFM Gd-O-Ti interactions are believed to be weaker than the ferromagnetic Ti-O-Ti interactions.¹² GdTiO₃ is just on the FM side of the FM-AFM

phase boundary; therefore, if the FM character is sensitive to octahedral rotations and distortions, significant effects on its magnetism with structural modifications may be expected.

In a previous study we have shown that approximately 1–3 GdO planes near the interface with SrTiO₃ exhibit a significant reduction in Gd displacements, and thus octahedral tilts, while in the interior of the GdTiO₃ layers these displacements agreed reasonably well with bulk values.¹⁹ Thus the need to maintain interfacial oxygen octahedral connectivity is mostly accommodated within the interfacial GdTiO₃. This suggests that by further decreasing the thickness of the GdTiO₃, the octahedral distortions in the entire GdTiO₃ layer can be modified.

GdTiO₃ films and GdTiO₃/SrTiO₃ superlattices were grown on (001) (La_{0.3}Sr_{0.7})(Al_{0.65}Ta_{0.35})O₃ (LSAT) by hybrid molecular beam epitaxy (MBE).^{20,21} A 20-nm GdTiO₃ film was grown directly on LSAT, while GdTiO₃ layers of 3.5, 2.4, and 2.0 nm thicknesses (ten, seven, and six GdO layers, respectively) were grown in a superlattice structure with 5 nm of SrTiO₃ spacers. Superlattices contained either five or ten GdTiO₃ layers, and thus approximately the same amount of GdTiO₃, by volume, as the 20-nm sample. They had 10-nm SrTiO₃ buffers and caps, respectively.

The magnetization was measured in a superconducting quantum interference device magnetometer (Quantum Design) with the magnetic field in the plane of the film. Cross-section transmission electron microscopy (TEM) foils were prepared by focused ion beam (5-kV Ga ions) and imaged using a field emission FEI Titan S/TEM with a super-twin lens ($C_s = 1.2$ mm) at 300 kV, using a 1024 × 1024 frame size and 30 μs dwell time. The convergence angle was 9.6 mrad. A deviation angle ($180^\circ - \theta$), was used to quantify the A -site (Gd, Sr) displacements, where θ is the angle between three successive A -site cations [see Fig. 1(a)]. A -site positions were determined from multiple high angle annular dark field (HAADF) images of each layer. Atomic centroid positions were extracted using a custom MATLAB algorithm.²² Orientation domains in GdTiO₃ are present (see Refs. 19 and 20). All images were taken along $[110]_O$, as A -site displacements can be discerned along this direction.¹⁹ While MBE provides near-monolayer thickness control, substrate miscut and surface steps cause uncertainties of ± 1 atomic plane in estimates of the layer thickness along the growth direction. The thicknesses given here represent the average number of atomic planes in TEM. Only images

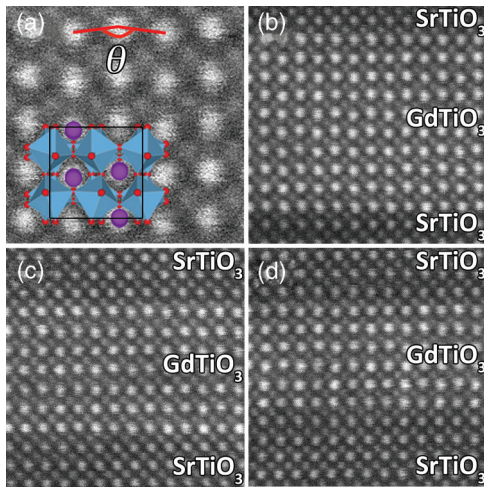


FIG. 1. (Color online) (a) HAADF-STEM image of a 20-nm GdTiO_3 film showing Gd displacements. The angle θ is measured between three successive Gd columns. A schematic of the unit cell is superimposed. (b)–(d) Representative images of 3.5-, 2.4-, and 2.0-nm-thick films.

of layers with the nominal thicknesses were selected for further analysis. Representative HAADF images of different GdTiO_3 thicknesses are shown in Fig. 1. Octahedral tilts were characterized using position averaged convergent beam electron diffraction (PACBED).^{17,23,24} PACBED patterns were recorded from areas of approximately four pseudocubic unit cells (slightly larger than the primitive orthorhombic unit cell projection), at the center of each GdTiO_3 film.

A-site cation displacements for each AO plane along the growth direction are shown in Fig. 2 for different GdTiO_3 thicknesses. Shaded areas indicate the GdTiO_3 layer, which can easily be identified from HAADF image intensities. The dashed line represents the average (~ 100 atomic rows over four images) deviation angle, $\sim 15^\circ$, of the 20-nm GdTiO_3 film, which matches that of bulk GdTiO_3 . As discussed elsewhere,¹⁹ SrO planes show no Sr displacements (the apparent deviation angle of $\sim 1^\circ$ is due to noise and instability, and serves as a measure of the error). About one to three GdO planes near

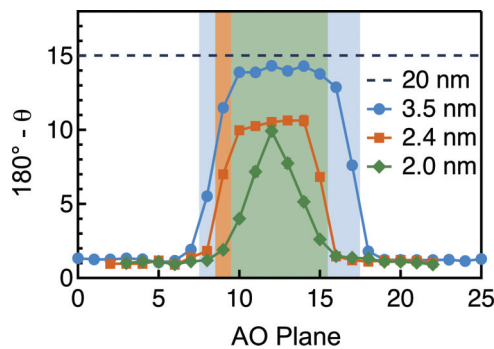


FIG. 2. (Color online) Deviation angles for each AO plane across $\text{SrTiO}_3/\text{GdTiO}_3/\text{SrTiO}_3$ interfaces with different GdTiO_3 thicknesses. The angle for the 20-nm film is indicated by the dashed line and is an average over ~ 100 GdO planes. Shaded regions indicate the extent of the GdTiO_3 film for each sample, determined from the HAADF image intensities.

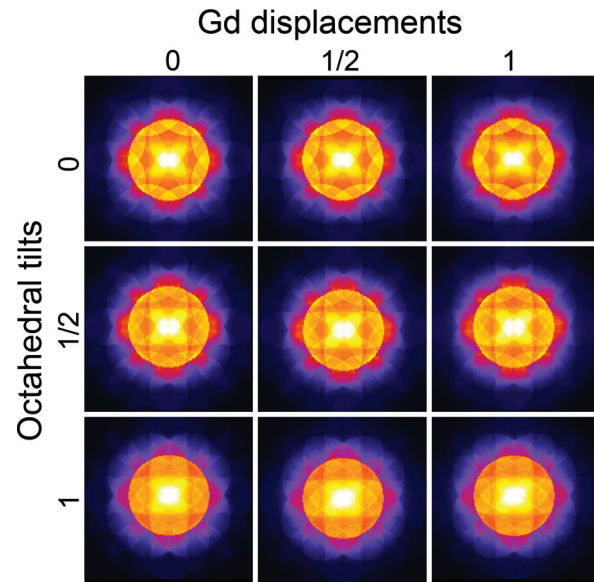


FIG. 3. (Color online) Simulated “ GdTiO_3 ” PACBED patterns for different Gd displacements and octahedral tilts (TEM foil thickness: 18.8 nm). The numbers indicate the degree of distortion, with 0 signifying no distortion, 1 the distortion in GdTiO_3 , and $\frac{1}{2}$ corresponding to the intermediate distortion. The top-left panel corresponds to the cubic structure, while the bottom-right panel is bulk GdTiO_3 .

the interface show reduced deviation angles in all samples, as discussed above. GdTiO_3 quantum wells of 3.5, 2.4, and 2.0 nm (ten, seven, and six GdO layers, respectively) show reduced deviation angles also *in the films' interior*, not just at the interface. For the 3.5- and 2.4-nm films, the deviation angle is constant at the center, slightly reduced from bulk for the 3.5-nm film ($\sim 14^\circ$), and with a significantly reduced value for the 2.4-nm film ($\sim 11^\circ$). In the 2.0-nm film, the deviation angle is $\sim 10^\circ$ in the center and then continuously decreases towards the interface.

To confirm that Gd displacements correlate with the octahedral tilts and distortions, as they do in bulk, PACBED was carried out. Figure 3 shows simulated $[110]_O$ PACBED patterns (Kirkland multislice code²⁵) for different octahedral tilts (rows) and Gd displacements (columns). It can be seen that the symmetry and features in PACBED are sensitive to the octahedral tilts, whereas the effects of Gd displacements are minor. Patterns without octahedral tilts (top row) show a dark concave octagonal shape, along with four “cross-shaped” regions within the central disk, while tilted patterns (bottom row) appear squarer, “lenslike” in the center and triangular corners. These features remain consistent regardless of Gd displacements. Figure 4 compares experimental and simulated PACBED patterns. For the simulations, the octahedral tilts and distortions are varied; the degree of distortion is based on the Gd-site displacements obtained from Fig. 2, and interpolation using bulk rare-earth data.¹² The top halves of the simulated patterns are convolved with a Gaussian function to account for the experimental point spread function and show good agreement with the experiment. As the octahedral rotations decrease, the GdTiO_3 PACBED becomes more “ SrTiO_3 -like,” (i.e., cubic).

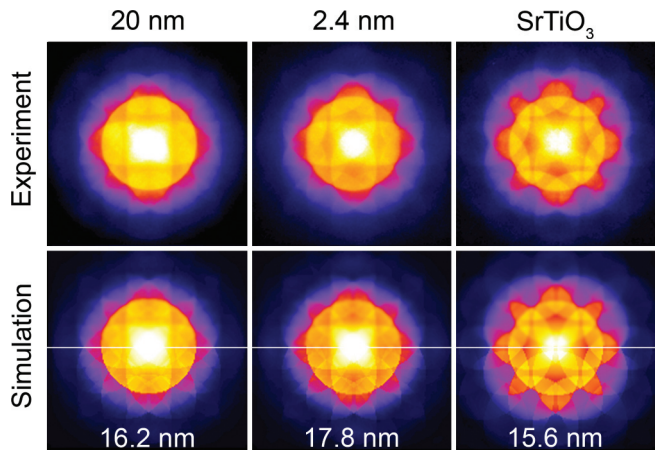


FIG. 4. (Color online) Experimental (top row) and simulated (bottom row) PACBED patterns of GdTiO₃ and SrTiO₃. White labels indicate the TEM foil thickness, and black ones the GdTiO₃ layer thicknesses from which the experimental data was acquired. Simulated patterns use the expected octahedral tilts from measured deviation angles. Gd displacements were taken to be bulklike for both GdTiO₃ simulations. The top half of simulated patterns include Gaussian convolution to account for detector point spread function, and show a better match to experimental patterns.

Figure 5(a) shows the magnetization of each sample as a function of temperature under a constant field of 100 Oe. The magnetization hysteresis at 2 K is shown in Fig. 5(b).

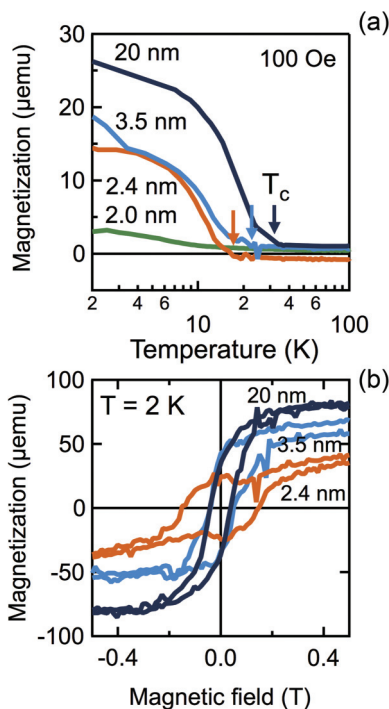


FIG. 5. (Color online) (a) Magnetization as a function of temperature for samples with GdTiO₃ films of various thicknesses recorded on cooling under a field of 100 Oe. The arrows indicate T_c . The data from the 19-nm sample is from Ref. 20. (b) Magnetization as a function of magnetic field at 2 K.

The measured magnetization includes the diamagnetic and paramagnetic responses from the SrTiO₃ layers, the LSAT, and a Ta backing layer. Although all samples were similar in size and contained comparable amounts of GdTiO₃, small size and thickness variations of substrate and backing layer are unavoidable. Isolating the GdTiO₃ response could not be done due to the superlattice structure. Therefore, conclusions about parameters that depend on the volume (saturation magnetization) should be made with care. The Curie temperature (T_c) and coercivity are, however, properties of only the FM GdTiO₃. The T_c of the 20-nm film (~ 30 K) agrees well with the bulk.^{12,13,18} All GdTiO₃ layers with thicknesses greater than 2.0 nm are FM, but their T_c decreases continuously with decreasing thickness (see arrows).

Comparing Figs. 2 and 5 reveals that the reduction in octahedral tilts causes a decrease in T_c . This behavior is expected by analogy with the bulk rare-earth titanates, which show a decrease in T_c with increasing bandwidth (reduced distortions), consistent with band ferromagnetism.²⁶ However, a quantitative comparison of film and bulk data reveals significant differences. Figure 6 shows the magnetic phase diagram as a function of deviation angle for thin films and bulk, respectively. In bulk, a transition from AFM to FM ordering occurs between Gd and Sm, at a deviation angle of $\sim 15^\circ$. In contrast, in the layers, the critical angle for FM behavior to vanish is $10.5 \pm 1^\circ$. This deviation angle is comparable to that of AFM LaTiO₃, which has the smallest GdFeO₃-type

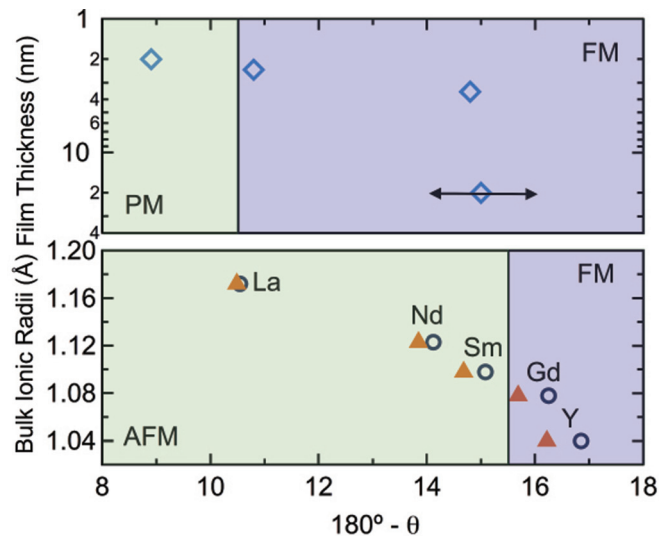


FIG. 6. (Color online) Measured deviation angles (open diamonds, top graph) for GdTiO₃ films with different film thicknesses. The FM stability region is indicated. The angles are an average of the center regions in the 3.5 and 2.4 nm quantum wells, and the peak value for the 2.0 nm quantum well. The arrow represents the estimated uncertainty of $\pm 1^\circ$, estimated from the SrTiO₃ deviation angle measurements, shown only on 20-nm film data for clarity, but applies to all measurements. The bottom graph (open circles) shows the deviation angles for bulk rare-earth titanates (Ref. 12) with different rare-earth ionic radii (Ref. 31). Filled triangles estimate the effects of coherent substrate strain and microscope scan asymmetry ($\sim 2\%$ difference between x and y directions, measured from cubic samples). Both change the measured lattice parameters and, hence, deviation angles. The FM and AFM stability regions are indicated.

distortion among all the rare-earth titanates, and is barely insulating.

The important conclusion is that FM ordering and anti-ferro-orbital ordering are not as strongly dependent on the orthorhombic distortion as may be implied from (naive) interpretation of the bulk phase diagram. Rather, the results support a picture of a direct interaction between orbital ordering—which determines the magnetism—and the lattice, somewhat independent from the degree of orthorhombic distortion. This interpretation is in agreement with recent reports of structural anomalies at the magnetic ordering temperature, which also support a direct lattice-orbital coupling.¹² Takubo and coauthors found that in the AFM rare-earth titanates, the orbital ordering changes at the ordering temperature, also suggesting a direct interaction.⁶ The FM rare-earth titanates thus appear to closely match models of narrow band, insulating, one-electron systems^{27–29} with a FM ground state. In these systems, antiferro-orbital ordering in conjunction with intra-atomic exchange results in ferromagnetism at a temperature below the orbital ordering temperature. The $4f^7$ configuration of the Gd ions ensures no orbital angular momentum contributions from the Gd, suggesting the interatomic exchange field—even at lower Ti-O-Ti bond angles—favors the FM ground state.

The FM ground state only vanishes in the 2.0-nm film that does not contain any continuous planes with the same Gd displacements (octahedral tilts) anymore. This may make long-range, coherent orbital ordering¹⁴ difficult, similar to what is observed in alloys such as $\text{La}_{1-x}\text{Y}_x\text{TiO}_3$ (Ref. 12) or $\text{Sm}_{1-x}\text{Gd}_x\text{TiO}_3$,²⁶ and may explain the vanishing T_c .

An open question that could not be answered is why deviation angles are already reduced in the interior of films that are still thicker than (twice) the thickness needed to accommodate the oxygen octahedral connectivity at the interface with SrTiO_3 . Theoretical simulations that consider long-range structural coherencies, as well as possible coupling with or between the high-density two-dimensional electron gases that are located at the interfaces in the SrTiO_3 (Ref. 30) may be needed to understand this.

Finally, we note that the results are consistent with the hypothesis that “magnetic dead layers,” widely reported for many perovskite films, are caused by interfacial structural distortions due to oxygen octahedral connectivity constraints. Suitably designed heterostructures (i.e., interfaces with smaller degrees of tilt mismatch) may be able to mitigate this.

The authors thank Leon Balents for many helpful discussions. The microscopy studies were supported by the DOE (Grant No. DEFG02-02ER45994). The magnetism studies were supported by a MURI program of the Army Research Office (Grant No. W911-NF-09-1-0398). J.Y.Z. received support from the Department of Defense through an NDSEG fellowship, and C.A.J. from the National Science Foundation through a Graduate Research Fellowship. Acquisition of the oxide MBE system used in this study was made possible through an NSF MRI grant (Award No. DMR 1126455). This work made use of facilities from the Center for Scientific Computing at the California Nanosystems Institute (NSF CNS-0960316) and the UCSB Materials Research Laboratory, an NSF-funded MRSEC (DMR-1121053).

*These authors contributed equally to this work.

¹M. Mochizuki and M. Imada, *New J. Phys.* **6**, 154 (2004).

²J. G. Cheng, Y. Sui, J. S. Zhou, J. B. Goodenough, and W. H. Su, *Phys. Rev. Lett.* **101**, 087205 (2008).

³J. B. Goodenough and J. S. Zhou, *J. Mater. Chem.* **17**, 2394 (2007).

⁴J. Akimitsu, H. Ichikawa, N. Eguchi, T. Miyano, M. Nishi, and K. Kakurai, *J. Phys. Soc. Jpn.* **70**, 3475 (2001).

⁵M. Itoh, M. Tsuchiya, H. Tanaka, and K. Motoya, *J. Phys. Soc. Jpn.* **68**, 2783 (1999).

⁶K. Takubo, M. Shimuta, J. E. Kim, K. Kato, M. Takata, and T. Katsufuji, *Phys. Rev. B* **82**, 020401 (2010).

⁷H. Nakao, Y. Wakabayashi, T. Kiyama, Y. Murakami, M. v. Zimmermann, J. P. Hill, Doon Gibbs, S. Ishihara, Y. Taguchi, and Y. Tokura, *Phys. Rev. B* **66**, 184419 (2002).

⁸R. Schmitz, O. Entin-Wohlman, A. Aharony, A. B. Harris, and E. Muller-Hartmann, *Phys. Rev. B* **71**, 144412 (2005).

⁹E. Pavarini, S. Biermann, A. Poteryaev, A. I. Lichtenstein, A. Georges, and O. K. Andersen, *Phys. Rev. Lett.* **92**, 176403 (2004).

¹⁰A. M. Glazer, *Acta Crystallogr., Sect. B: Struct. Crystallogr. Cryst. Chem.* **28**, 3384 (1972).

¹¹P. M. Woodward, *Acta Crystallogr., Sect. B: Struct. Sci.* **53**, 44 (1997).

¹²A. C. Komarek, H. Roth, M. Cwik, W. D. Stein, J. Baier, M. Kriener, F. Bouree, T. Lorenz, and M. Braden, *Phys. Rev. B* **75**, 224402 (2007).

¹³H. D. Zhou and J. B. Goodenough, *J. Phys.: Condens. Matter* **17**, 7395 (2005).

¹⁴M. Kubota, H. Nakao, Y. Murakami, Y. Taguchi, M. Iwama, and Y. Tokura, *Phys. Rev. B* **70**, 245125 (2004).

¹⁵E. Pavarini, A. Yamasaki, J. Nuss, and O. K. Andersen, *New J. Phys.* **7**, 188 (2005).

¹⁶J. M. Rondinelli, S. J. May, and J. W. Freeland, *MRS Bull.* **37**, 261 (2012).

¹⁷J. Hwang, J. Son, J. Y. Zhang, A. Janotti, C. G. Van de Walle, and S. Stemmer, *Phys. Rev. B* **87**, 060101 (2013).

¹⁸C. W. Turner and J. E. Greedan, *J. Solid State Chem.* **34**, 207 (1980).

¹⁹J. Y. Zhang, J. Hwang, S. Raghavan, and S. Stemmer, *Phys. Rev. Lett.* **110**, 256401 (2013).

²⁰P. Moetakef, J. Y. Zhang, S. Raghavan, A. P. Kajdos, and S. Stemmer, *J. Vac. Sci. Technol. A* **31**, 041503 (2013).

²¹B. Jalan, R. Engel-Herbert, N. J. Wright, and S. Stemmer, *J. Vac. Sci. Technol. A* **27**, 461 (2009).

²²J. M. LeBeau and S. Stemmer, *Ultramicroscopy* **108**, 1653 (2008).

²³J. M. LeBeau, S. D. Findlay, L. J. Allen, and S. Stemmer, *Ultramicroscopy* **110**, 118 (2010).

²⁴J. Hwang, J. Y. Zhang, J. Son, and S. Stemmer, *Appl. Phys. Lett.* **100**, 191909 (2012).

²⁵E. J. Kirkland, *Advanced Computing in Electron Microscopy* (Springer, New York, 2010).

- ²⁶G. Amow, J. S. Zhou, and J. B. Goodenough, *J. Solid State Chem.* **154**, 619 (2000).
- ²⁷L. M. Roth, *Phys. Rev.* **149**, 306 (1966).
- ²⁸S. Inagaki, *J. Phys. Soc. Jpn.* **39**, 596 (1975).
- ²⁹D. I. Khomskii and K. I. Kugel, *Solid State Commun.* **13**, 763 (1973).
- ³⁰P. Moetakef, T. A. Cain, D. G. Ouellette, J. Y. Zhang, D. O. Klenov, A. Janotti, C. G. Van de Walle, S. Rajan, S. J. Allen, and S. Stemmer, *Appl. Phys. Lett.* **99**, 232116 (2011).
- ³¹R. D. Shannon, *Acta Crystallogr., Sect. A: Cryst. Phys., Diffraction. Gen. Crystallogr.* **32**, 751 (1976).